ACS OMEGA

Open Access

http://pubs.acs.org/journal/acsodf

Article

Synthesis of Cross-Linked and Sterilized Water-Soluble Electrospun Nanofiber Biomatrix of Streptomycin-Imbedded PVA/CHN/β-CD for Wound Healing

Mohamed Mohsen, Sara A. Abdel Gaber, Kamel R. Shoueir,* Maged El-Kemary, and Wafaa S. Abo El-Yazeed*

Cite This: *ACS Omega* 2024, 9, 10058−10068

Read Online

ACCESS | Metrics & More | Article Recommendations

ABSTRACT: The diagnosis and prognosis of chronic wounds are demanding and require objective assessment. Because of their potential medicinal applications, the syntheses of biopolymeric chitosan (CHN) structure and PVA-based mixed electrospun nanofibers with biomimetic features were thoroughly investigated. This study created different formulas, including a guest molecule and capping agent, using supporting PVA as a vehicle. CHN was used as a biomodifier, and beta-cyclodextrin (ß-CD) as a smoother and more efficiently entraps streptomycin (STP) compared with the silver sheet wound dressing. The relevant analyses showed that the size distribution increased with the incorporation of PVA, CHN, and ß-CD to 120.3, 161.9, and 192.02 nm. The webs boosted particle size and released content stability to 96.4% without compromising the nanofiber structure. Examining the synergistic effects of the PVA/CHN/STP/ß-CD nanoformulation against pathogenic strains of *S. aureus*, *P. aeruginosa*, and *Aspergillus niger*, clean zones were 47 ± 3.4, 45 ± 3.0, and 49 ± 3.7 mm were produced. PVA/CHN/STP/ß-CD formula exhibited a 98.9 ± 0.6% cell viability and wound closure of 100% at 72 h. The results reveal that the PVA/CHN/STP/ß-CD formula is promising for medical applications, especially in wound healing, compared with the silver sheet.

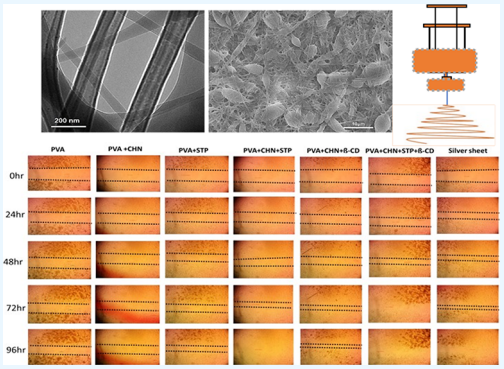

1. INTRODUCTION

Skin is an essential organ of the human body, serving as a protective barrier against external risk factors that may create adverse consequences; thus, it is regarded as the first line of defense in protecting the human body.[1,2] Electrospun nanofibers exhibit high pores, large surface area, and 3D structure, which render such materials promising for biological applications to protect skin from external attack.[3−5] Electrospun nanofibrous mats with a natural extracellular matrix modeling (ECM) structure can promote adhesion and proliferation in water, primarily as a long-term barrier to bacterial colonization,[6] super exudate absorbers,[7] oxygen filters, and vapor penetration.[8]

To ensure minimal side effects, controlled medications from various periods are precisely administered to the specific target area.[9] Among solvents, water stands out as the optimal choice for electrospinning nanofibers due to its nontoxicity, cytocompatibility, and universal applicability.[10,11] The skin acts as a crucial barrier against microbes; therefore, any skin injury demands appropriate wound care for hemostasis, healing, and safeguarding the body from external elements.[12,13] Wound dressing materials must meet stringent criteria; they should be nontoxic, nonallergenic, and create a conducive environment for accelerated wound healing. Additionally, an ideal wound dressing should possess antibacterial properties to facilitate the healing of infected wounds.[14−17]

It was proved that electrospun nanofiber scaffolds comprised biopolymers have excellent physicochemical properties, including superior mechanical and thermal properties, and minimize biopolymers' degradation.[18−20] Chitosan (CHN) is a natural biopolymer (biodegradable and biocompatible) prepared by the deacetylation of chitin. CHN has many different applications and comprises tissue engineering,[21] wound dressing,[22,23] antibacterial,[24] stem cells,[25] wastewater treatments,[26] and others.[27−29] It offers advantages in nanofibrous dressing since it reduces costs and high efficiency. However, certain disadvantages exist, such as low mechanical properties and weak thermal stability. Besides, the polycationic

Received: May 7, 2023
Revised: December 23, 2023
Accepted: February 12, 2024
Published: February 26, 2024

Table 1. Compositional Form of Nanofiber Formulations in the Present Protocol

nanofibers series	PVA/CHN/β-CD (wt %)	STP (%wt./v)	viscosity (cP)	diameter ± SD (nm)
PVA	100:0:0		301	120.32 ± 35.9
PVA@STP	100:0:0	5	298	
PVA/CHN	90:10:0		335	161.92 ± 25.21
PVA/CHN@STP	90:10:0	5	334	
PVA/CHN/β-CD	80:10:10		320	299.14 ± 31.58
PVA/CHN/β-CD@STP	80:10:10	5	316	

structure of CHN causes its solution to be extremely viscous, making electrostatic spinning challenging.[28] By combining CHN with other synthetic biocompatible polymers such as poly(vinyl alcohol) (PVA), these limitations can be overcome.[9,10,30] PVA has many beneficial properties, including its ability to form fibers, degrade quickly, and absorb moisture. PVA nanofibers can absorb the exudates in infected wounds and enhance the regeneration of wound tissues due to their nontoxicity, biocompatibility, and oxygen permeability.[31] Cyclodextrin (CD) was recommended as a biopolymer to modify PVA and CHN to improve the solubility and electrospinnability for producing a smart drug carrier. The FDA has approved CD,[32] and its supramolecular structure allows it to be electrospun in water without any additional polymer.[33] The versatile process of complexation with Cyclodextrins (CDs) allows for the integration of the unique physicochemical characteristics of guest compounds. The CD also improved the spinning stability during the interaction with PVA, as published elsewhere.[34] Otherwise, CD's cone shape has a hydrophobic inner chamber and a hydrophilic outer surface that facilitates the formation of noncovalent supramolecular inclusion complexes with a range of substances.[35] Because of their complexation capabilities, CD cavities improve drug solubility because they diffuse easier than free drugs.[36]

The choice of an appropriate antibiotic for local delivery devices is critical. The selected antibiotic must be efficient against germs while still being biocompatible with tissue. Streptomycin (STP), a common aminoglycoside antibiotic, was used as a proof of concept. Despite being the first antibiotic shown effective against *Mycobacterium tuberculosis*, STP has lost popularity due to resistance. In multidrug-resistant tuberculosis, it is recommended as a supplementary therapy.[37]

The current research aimed to prepare different nanoformulations based on PVA nanofibers and then employed mixed electrospinning with CHN and β-CD. Using STP as a model drug molecule, the unique properties of PVA/CHN/β-CD nanofibers as a drug delivery system were investigated and compared to those of a commercial silver sheet wound dressing.

2. METHODOLOGY

2.1. Materials and Reagents. PVA (87−90% hydrolyzed, M_w 30,000−70,000), poly(D-glucosamine), CHN (medium MW), β-CD (purity ≥97%), and glutaraldehyde solution were purchased from Sigma-Aldrich Co. (Germany). Broad-spectrum aminoglycoside STP ($C_{21}H_{39}N_7O_{12}$) was provided by PubChem, India. Without further purification or modifications, all other chemicals were used as received.

2.2. Preparation of Electrospun Polymer Solution and Cross-Linking Method. Viscous PVA solution was prepared by dissolving 10 g in 100 mL of double distilled water for 4 h at 80 °C under vigorous mechanical stirring. On the other hand, CHN (1% w/v) was dissolved in a glacial acetic acid solution to obtain an off-white solution. In parallel, β-CD (1 g) was dissolved in an aqueous water solution (100 mL). After that, the nonequal ratios were mixed as set in Table 1 to form the nominated admixtures: PVA/STP, PVA/CHN@STP, and PVA/CHN/β-CD@STP.

Then, for the electrospinning process, 10 mL of the polymer solutions (PVA, PVA/CHN, and PVA/CHN/ β-CD) with and without STP were placed into a syringe pump. The experiments used the following parameters: 26 kV, 0.1 mm/h feed rate, the approximated distance between charged collector and Taylor cone was 12 cm, and the needle diameter was 18 φ. A cleaning process every 30 min was required to prevent needle blockage.

After 40 h at room temperature, the nanofibers were separated from aluminum foil. All nanofibers were immersed in a 200 mL admixture of absolute ethanol and water solution comprising NaOH (1.5 g) and 20% glutaraldehyde (2 mL) for 2 h, acting as cross-linking agents for the formed nanofibers. Finally, the nanofibers were vacuum-dried until analysis.

2.3. UV Curing for Sterilization and Stability of Nanofibers. Following electrospinning, the sterilized system consists of a handmade setup ultraviolet reactor. The designed system includes 4 UV lamps (4 × 8 W) used for sterilization (λ = 265 nm, Hitachi, Japan). The nanofibers were placed in the cabinet reactor; UV-irradiation light was focused from both sides, and the light was equally distributed to ensure good sterilization for patches. The stability of the nanofibrous webs was evaluated for 7 days at 10 °C and room temperature with a relative humidity of 70%.

2.4. Characterization. Fourier-transform infrared spectroscopy (FTIR, JASCO FTIR-4X) was used to define the functionality and interaction between nanofibers. A digital viscometer RM 100p is used to measure the resistance of liquids to flow before electrospinning. Surface morphology, shape, size, and texture were recognized by transmission electron microscopy (TEM, JEOL, 1200). The surface morphologies were evaluated using high-field scanning electron microscopy (FE-SEM, QUANTA FEG250). In addition, a dispersive energy X-ray (EDX) was used to determine the elemental analysis of the selected samples. For the wound dressing assay, an inverted microscope was used (Motic AE31 Inverted Biological Microscope).

2.5. Detection of Drug Entrapment Capacity. The drug entrapment capacity (*E*%) of nanofibers comprised PVA/CHN/β-CD was measured using an ultrafiltration procedure. About 1.5 × 1.5 cm, 100 mg of the prepared PVA/CHN/β-CD nanofibers were placed onto a Millipore UFC910024 Amicon Ultra Centrifugal Filter with a 15 mL capacity and a 100 kDa pore size and centrifuged at 50 rpm for 30 min. At λ_{max} = 237 nm, the amount of physically adsorbed STP in the supernatant was measured spectrophotometrically. The physical unbound

https://doi.org/10.1021/acsomega.3c03146
ACS Omega 2024, 9, 10058−10068

STP concentration values were detected using the regression equation $Y = 0.05X + 0.0029$, with a correlation coefficient $R^2 = 0.998$, and compared to a previously published calibration curve of STP in water at varying concentrations ranging from 10 to 40 g/mL. Three times were acquired to replicate the proposed test, and the encapsulation efficiency of STP-loaded PVA/CHN/β-CD was calculated using the following formula:

$$E(\%) = \frac{D_1 - D_0}{D_0} \times 100 \quad (1)$$

where $E\%$ is the loading efficiency, D_1 is denoted as the starting amount of STP, and D_0 is the unbounded STP.

2.6. In Vitro Release Study. The release behavior was investigated using PBS at two different pHs: 5.0 and 7.4. The resulting PVA/CHN/β-CD@STP nanofiber (1.5 × 1.5 cm; 100 mg) was soaked in 15 mL of the PBS as mentioned earlier and dialyzed against 20 mL of PBS at 37 °C for 2 days in a shaking incubator at 50 rpm under dark conditions utilizing a dialysis bag with a porosity of 8000 to 14,000 Da. The release medium was removed and replaced with a new medium at specific intervals. From the standard curve of STP as a reference, the absorbance was detected precisely at λ_{max} 237 nm at time intervals. The following formula was used to calculate the release fraction from PVA/CHN/ β -CD@STP:

$$\text{LD cumulative release}(\%) = \left(\frac{A_t}{A_v}\right) \times 100 \quad (2)$$

where A_t is the amount of released STP from PVA/CHN/β-CD nanofibers at a predetermined time (A_t), and A_v is the amount of STP previously loaded inside PVA/CHN/β-CD nanofibers.

2.7. Antimicrobial Activities Using the Agar Disk Diffusion Method. Sample discs (1 cm in diameter) were inserted on nutrient agar plates spreader with test microorganisms and cultured for 24 h at the proper temperature for every test organism. Bacteria were cultivated on nutritional agar, while the fungi were cultured on potato dextrose agar (PDA). Each microbe culture was diluted to 1×10^7−10^8 CFU/mL in sterile distilled water. The inoculated agar plates were chilled for 2 h before incubating for 24 h at 37 °C for (yeast and bacteria) and 48 h at 30 °C for fungi. After incubation, the diameter of inhibitory zones against test microorganisms was determined. G-positive bacteria (*S. aureus* ATCC6538-P), G-negative bacteria (*P. areuginosa* ATCC27853), yeasts (*Candida albicans* ATCC10231), and the fungus (*Aspergillus niger* NRRL A-326).[38,39]

2.8. Cell Viability Assay. The human skin fibroblast (HSF) cells were seeded in Dulbecco's modified Eagle medium (DMEM) medium supplied with 10% fetal bovine serum and 100 U/mL penicillin in addition to 100 μg/mL/STP mixture and incubated in a 5% CO_2 incubator for 24 h at 37 °C. Cell viability was determined via the sulforhodamine B (SRB) test. 100 μL of suspended cells (5×10^3 cells) were incubated for 24 h in 96-well plates. Another quantity of (100 μL of media) was given to the cells containing our candidate formulas, and cells were fixed for 72 h; then, the medium was replaced with 100 μL of (10% TCA) and fostered at 4 °C for 1 h. After the TCA solution was eliminated, cells were washed 3 times with D.W. Afterward, 70 μL of SRB solution (0.4% w/v) was mixed and left at RT for 10 min in the dark. Plates were cleaned 3 times with 1% acetic acid and air-dried for 24 h. The protein-bound (SRB) stain was then solubilized in 150 μL of TRIS (10 mM), and the optical density was recorded at 540 nm via (the BMG LABTECH-FLUO star Omega microplate reader, Ortenberg, Germany).[40,41]

2.9. Wound Healing Methodology. *2.9.1. Wound Dressing Assay.* For the scratch wound evaluation, HSF cells were seeded in 5% FBS-DMEM and plated onto a coated 6-well plate at 3×10^5/well density, then cultivated overnight in a 5% CO_2 incubator at 37 °C. The next day, the confluent monolayer was horizontally scratched; the plate was scrubbed entirely with PBS; the control wells were refilled with fresh medium, and drug wells were treated with new media possessing the drug. At the stated time intervals, graphs were taken by an inverted microscope. The plate was cultivated in a 5% CO_2 incubator at 37 °C. The accepted photographs are shown below and can be evaluated as follows.

2.9.2. Wound Area and Wound Closure %. The wound area can be determined by tracing the cell-free area in images using the free Fiji-ImageJ program (NIH, Bethesda, MD).[42] Under normal circumstances, the wound area will shrink all of the time. The wound closure (%) can be stated as the percentage of wound closure area decreasing, which rises as cells constantly move.

$$\text{Wound closure}(\%): (0\text{ h} - \Delta h/0\text{ h}) \times 100 \quad (3)$$

where 0 h is the average wound area computed immediately after scratching (time zero) and Δh *is* the average wound area computed hours after the scratch is performed.

2.10. Statistical Evaluation. The data were collected in triplicate and represented as mean, standard deviation (SD, $n = 3$). The analysis of variance (ANOVA) was used to identify the significant difference analysis using IBM SPSS Statistics 1.0.0−2482. The statistically significant bar was set at $P < 0.05$.

3. RESULTS AND DISCUSSION

This work aims to load pharmaceutical drugs (STP) on different polymers, individually or blended, in the form of nanofibers. Therefore, polymers of various functions such as PVA, a synthetic polymer with an aliphatic structure, were used. At the same time, CHN is a branched carbohydrate polymer that contains different functional groups (−OH and $-NH_2$ groups) than PVA (−OH groups). The third polymer, β-CD, has a different nature and contains hydrophobic cavities in addition to huge −OH groups. The morphological structure, average diameter size, and loading efficiency of the produced nanofibers with these polymers can be varied. Thus, the following comprehensively characterizes the preparation of nanofibers loaded with STP as a model drug.

Table 1 depicts the different compositions of PVA, CHN, and β-CD with and without STP. STP was blended with a PVA, PVA/CHN, and PVA/CHN/ β-CD solution in our designed work. These different formulas have an impact factor on the viscosity of the produced solutions. Taking into account that the mixed solutions were kept under vigorous stirring until complete homogeneity before the electrospinning step. It can be observed from Table 1 that the PVA solution has a viscosity value equal to 301 cP.

Meanwhile, the value of PVA viscosity was sharply increased by adding CHN solution.[43] As is well-known, CHN solution has a considerable molecular weight. It is also a branched polymer that forms a viscous solution and increases the viscosity of PVA (335 cP). On the other hand, β-CD has a low molecular weight and causes a decrement in the viscosity value of the whole solution (320 cP). It is also depicted from the

https://doi.org/10.1021/acsomega.3c03146
ACS Omega 2024, 9, 10058−10068

viscosity assessment for the prepared solutions that STP has a neglected impact on the viscosity of PVA, PVA/CHN, and PVA/CHN/ β-CD.

3.1. FTIR of the Fabricated Nanofibers. For more illustration, the molecular interaction of PVA, CHN, β-CD, and STP in the produced nanofibers was studied through FTIR analysis (Figure 1). A broad absorption peak at 3237 cm^{-1} was

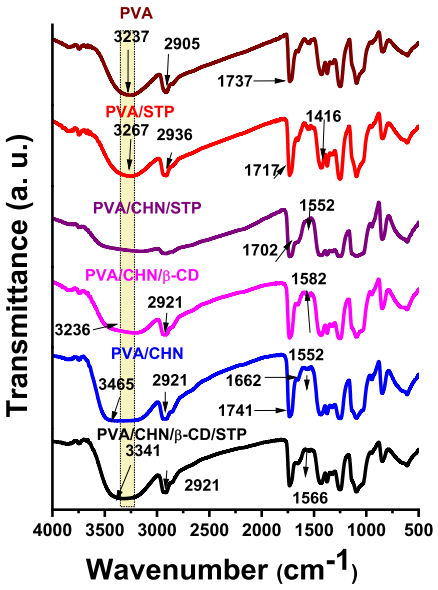

Figure 1. FTIR spectrum of designed nanofibers before and after loading of STP.

assigned to the stretching frequency of −OH groups, while 2905 cm^{-1} was attributed to the presence of asymmetric vibration of C−H groups of pure PVA nanofibers.[44] The peak appeared at 3465 cm^{-1} ascribed to stretching vibration of N−H and O−H bonds, 1662 cm^{-1} for the stretching C═O (amide I), 1552 cm^{-1} for N−H bending (amide II), are the key characteristic bands for CHN.[24,27,45] The hydrogen bonding interaction between reactive amine and hydroxyl functional groups of CHN and hydroxyl groups of PVA was observable in the FTIR spectra of CHN/PVA mixed nanofibers, with a few peaks overlapped. The incorporation of PVA into CHN leads to a notable enhancement in hydroxyl groups, evident in the shift of the −OH band from 3237 to a wide 3465 cm^{-1}. There is a discernible increase in the presence of −CH groups from 2905 to 2921 cm^{-1} and the emergence of carbonyl groups at 1741 cm^{-1}. Consequently, the bonding mechanism primarily involves the hydroxyl groups of PVA, along with the hydroxyl (predominantly) and amino groups of CHN. This is supported by the characteristic N−H band at 1572 cm^{-1}, which diminishes and shifts to 1545 cm^{-1}, indicating their significant involvement in the bonding interactions. Regarding FTIR of CD, the O−H stretching vibrational modes corresponding to distinct −OH groups (primary and secondary groups) and HOH are detected in the 3500−3000 cm^{-1} range and the C−H stretching bands appeared at 2921 cm^{-1}.[46] In the literature, the STP's typical peaks are 2352 and 2364 cm^{-1} due to C−O, C═C stretching, and 1969 cm^{-1} due to −OH stretching.[47] Infrared investigations revealed that the −C═O, −OH, and −NH groups make up the majority of STP functional group assignments. These functional groups overlapped with the nanofibers polymers and may be attributed to the total encapsulation of STP into the polymer's matrix.

3.2. TEM Analysis. TEM micrographs provided crucial insights into the morphology of the produced nanofibers, in both the presence and absence of STP loading. The images of PVA/CHN/β-CD and PVA/CHN/β-CD@STP samples, as shown in Figure 2a,b, revealed distinct features. PVA/CHN/β-CD nanofibers appeared as thin fibers with uniform, faint color throughout. In contrast, Figure 2c displayed the TEM image of PVA/CHN/β-CD@STP, showcasing dark zones amid faint colors. These darker regions can be attributed to the encapsulation of STP within the polymer nanofibers. Moreover, the TEM images (Figure 2c) highlighted the successful anchoring of STP onto the PVA/CHN/β-CD, indicating the formation of multiple nanonetwork structures within the material. This observation underscores the effective incorporation and distribution of STP within the nanofibers.

3.3. SEM, EDX, and Mapping. The morphological structures formed from all these prepared solutions (PVA, PVA/CHN, and PVA/CHN/ β-CD) can be observed in that the nanofibers without drugs have entirely different morphological features than those loaded with STP (Figure 3). As defined, nanofibers have a vast surface area and a porous structure capable of encapsulating STP drugs. From Figure 3a, it can be depicted that PVA nanofibers have a smooth surface, free bead fibers, and length fibers. The average diameter of the PVA nanofibers was around 120.32 nm (Figure 3d). By adding CHN to the PVA solution, the surface structure of the produced nanofibers is still with no difference, no noticeable for the beads or shorted fibers (Figure 3b). Thus, the addition of CHN to PVA has no significant impact on the morphological feature, except for the insignificant increase in the fiber diameter (161.92 nm; Figure 3e). On the contrary, β-CD harms the surface of PVA/CHN nanofibers (Figure 3c). β-CD leads to the formation of nanofibers that are noticeably collected with poor porosity and a large diameter of 192.02 nm according to the size distribution (Figure 3f) due to the

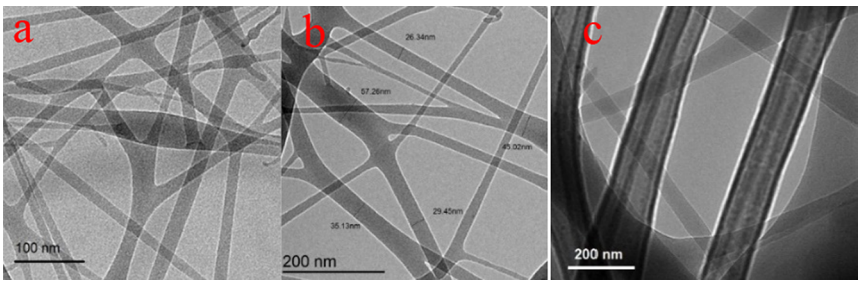

Figure 2. TEM of (a, b) PVA/CHN/β-CD at two different magnifications and (c) PVA/CHN/β- CD@STP.

https://doi.org/10.1021/acsomega.3c03146
ACS Omega 2024, 9, 10058−10068

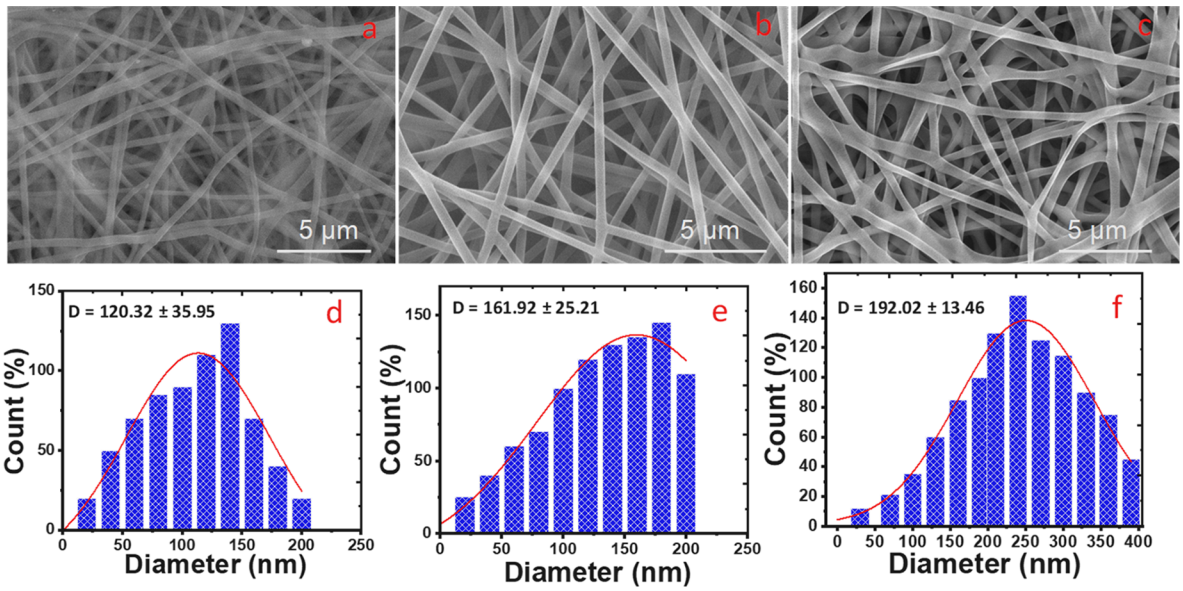

Figure 3. SEM of (a) PVA, (b) PVA/CHN, (c) PVA/CHN/β-CD, and the size distribution of (d) PVA, (e) PVA/CHN, and (f) PVA/CHN/β-CD nanofibers.

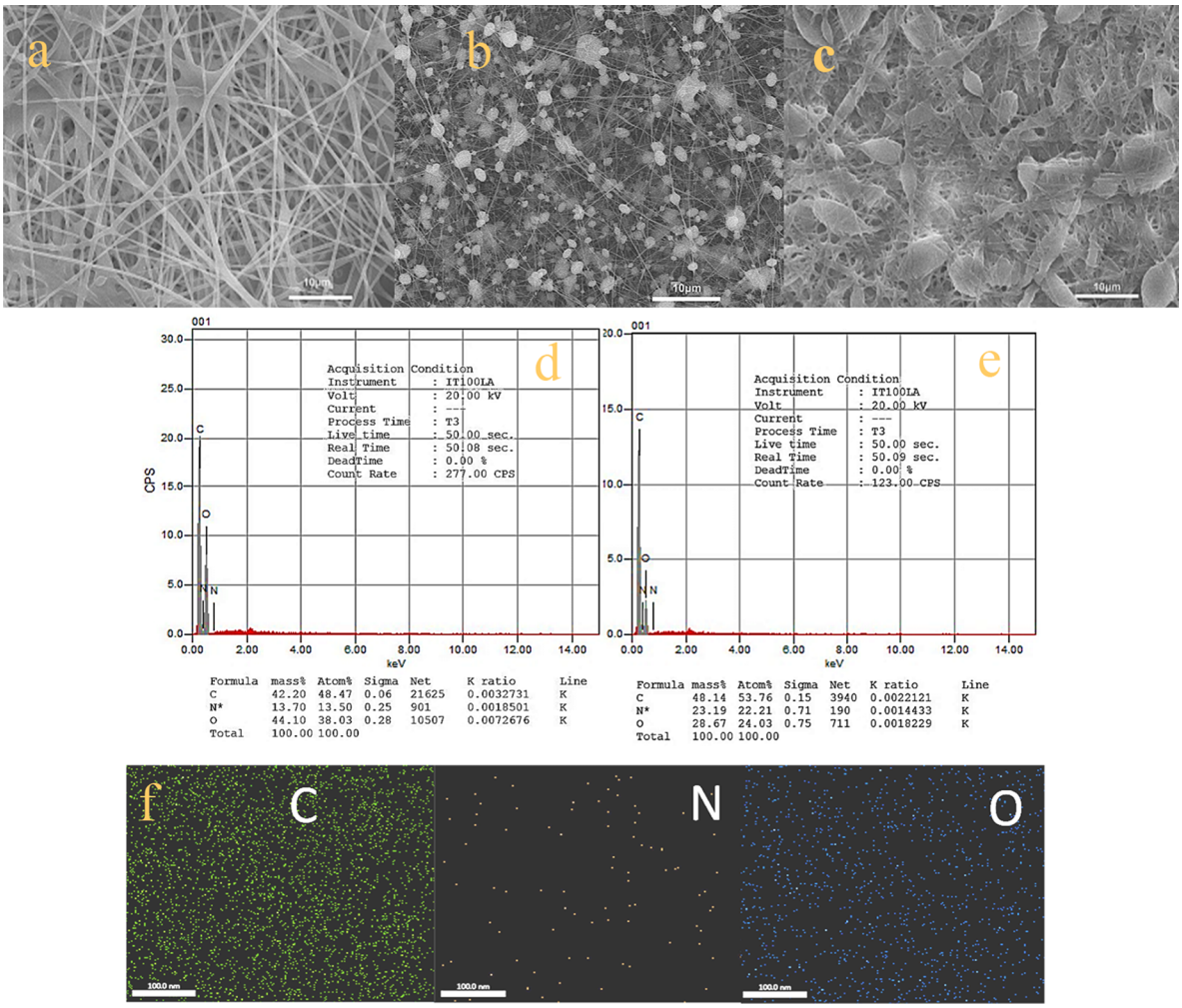

Figure 4. SEM of drug interaction of (a) PVA@STP, (b) PVA/CHN@STP, (c) PVA/CHN/β-CD@STP, and EDX analysis of (d) PVA/CHN/β-CD and (e) PVA/CHN/β-CD after loading of STP (PVA/CHN/β-CD@STP). Mapping analysis of (f) C, N, and O elements in the neat nanofibers.

https://doi.org/10.1021/acsomega.3c03146
ACS Omega 2024, 9, 10058−10068

formation of fused fibers with each other (Figure 3c). That is because β-CD cannot form homogeneous nanometer fibers (weak electrospinning),[18,48] in addition to its low viscosity and its inability to strongly homogenize with CHN, which is deposited in the form of points on the surface of the formed fiber.

Figure 4a displays the nanofibers from the PVA solution blended with STP. It is shown that the nanofibers still have a smooth surface area but with little cluster particles deposited on the surface of PVA, which could be assigned to the deposition of STP. While the behavior of STP is different with PVA/CHN nanofibers (Figure 4b) as well as some STP is deposited onto the surface of the nanofibers in small spherical particles. This small particle can be entered easily into the porous structures of the nanofibers. Compared with neat PVA nanofibers, CHN has huge $-NH_2$ and $-OH$ groups in its backbone and contributes to capturing many of the added drugs (STP).[49] Next, PVA/CHN/ β-CD loaded with STP (Figure 4c) has an ultimate surface structure. The appearance of beads beside the nanofiber's formation can be assigned to the hydrophobic cavities of β-CD that facilitate STP incorporation into these cavities.[50]

Hence, β-CD containing STP is deposited on the nanofibers of the mixture of CHN and PVA in the form of relatively large particles. Regardless of the shape and surface of nanofibers, the STP amount is relatively large, which is attributed to the mixing property of β-CD next to CHN and mixing them in a new formula with PVA.[51−53]

To confirm and deepen the preparation of the nanofibers, the selected samples (PVA/CHN/β-CD and PVA/CHN/β-CD@STP) were characterized using EDX to identify the elements into structures. Thus, Figure 4d,e illustrates the graphs that originated from EDX analysis. It is observed that the two samples contain C, O, and N elements. All the chemical compounds (PVA, CHN, β-CD, and STP) used for nanofiber formation have these elements, but the only difference is that the percentage of nitrogen was increased when these polymer solutions were loaded with STP. Figure 4f illustrates the mapping images demonstrating the dispersion of each element that comprises the nanofibers loaded with STP.

3.4. In Vitro Detection of Drug Loading and Release Study. Upon rigorous examination and meticulous analysis, the drug loading capacity and encapsulation efficiency were thoroughly determined, unveiling remarkable values of 81.3 and 90.8%, respectively. This meticulous assessment highlighted the robustness of the drug encapsulation process, showcasing high efficacy in loading the intended drug and ensuring its effective encapsulation within the carrier system. Figure 5 illustrates the release kinetics of STP (μg/mL) from PVA/CHN/β-CD@STP. Notably, the controlled release of STP at pH 7.4 (8.5 μg/mL) over 260 min closely resembled the release profile observed at pH 5.5 (5.5 μg/mL). It is essential to acknowledge that the soluble nature of CHN at lower pH values contributed to the favorable CHN-released profile at pH 5.5.[54,55] The accelerated release (%) observed in PVA/CHN/β-CD@STP can be attributed to its more concentrated polymeric chain, featuring porous structures, smaller fiber diameter, and shorter distances that facilitate rapid diffusion of STP, thereby expediting its release.[37,47,56]

3.5. Cytocompatibility. The cytocompatibility assay was accomplished with HSF cell lines. The result obtained by the SRB assay (Figure 6) demonstrated that nanofibrous scaffolds originating from PVA exhibit relatively high cell viability values

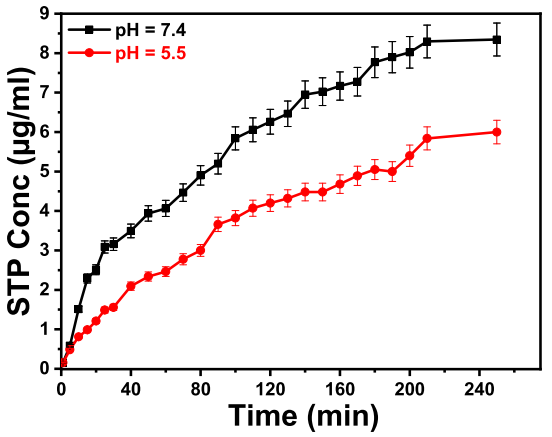

Figure 5. STP release profile for PVA/CHN/β-CD@STP at pH 7.4 and 5.5.

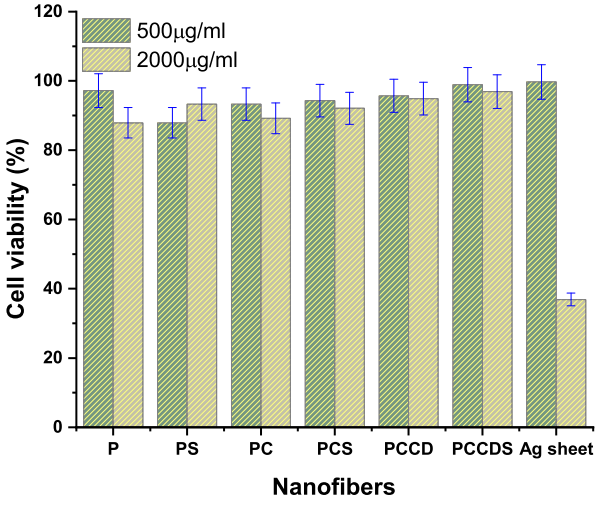

Figure 6. Cell viability of nanofibers and Ag sheet control at low and high concentrations.

(97.2 ± 1.1%) at 500 μg/mL and (87.9 ± 0.1%) at 2000 μg/mL, while the cell viability of all fabricated nanofiber formulas was near or the same to PVA nanofiber as listed in Table 2. In the case of the Ag sheet, the cell viability declined at higher concentrations until 36.9 ± 1.6%, which indicates that the presence of silver nanoparticles (AgNPs) could be incorporated in the cell membrane and decrease its viability, which makes it not appropriate for medical applications compared to our candidate formulas. It is known that silver nanoparticles release lethal reactive oxygen species and silver ions that could elucidate cellular toxicities at both the in vitro and in vivo levels. It can be illustrated that there is no significant decrease in viable cells within PVA, PVA/STP, PVA/CHN, PVA/CHN/β-CD, and PVA/CHN /ß-CD/ STP. Based on that, it can be reported that our candidate formulas are nontoxic, safe, and cell-compatible and can be used as a biomaterial for wound healing. Such obtained data agree with the recent study in which the fabricated PVA-based nanofiber was used as a carrier of gold nanoparticles (AuNPs). AuNPs synthesized using carboxymethyl chitosan show good cell viability with 96.1 ± 0.3% for higher doses.[57]

3.6. Antibacterial Activity. Human wound fluids are an ideal environment for the growth of pathogenic bacteria that encourage illnesses and hinder healing.[58,59] It is expected that

https://doi.org/10.1021/acsomega.3c03146
ACS Omega 2024, 9, 10058−10068

Table 2. Cell Viability of All Formulas at 500 and 2000 μg/mL

		cell viability %						
nanofiber		PVA	PVA/STP	PVA/CHN	PVA/CHN/STP	PVA/CHN/β-CD	PVA/CHN/β-CD@STP	Ag sheet
conc. (μg/mL)	500	97.2 ± 1.1	97.9 ± 1.5	93.0 ± 0.2	94.3 ± 0.2	95.7 ± 0.4	98.9 ± 0.6	99.7 ± 0.1
	2000	87.9 ± 0.1	93.3 ± 0.7	89.2 ± 0.2	92.1 ± 0.3	94.9 ± 0.2	96.9 ± 0.7	36.9 ± 1.6

Table 3. ZOI (ϕmm) of Our Six-Nanofiber Formula Compared with Silver Sheet against Bacteria, Fungi, and Yeast

		clear zone (ϕ mm)			
no	sample	*S. aureus*	*P. aeruginosa*	*A. niger*	*C. albicans*
1	PVA	18 ± 2.1	11 ± 1.3	10 ± 0.9	0
2	PVA/CHN	15 ± 1.9	16 ± 1.4	22 ± 1.1	0
3	PVA/STP	46 ± 2.0	44 ± 2.8	43 ± 1.4	0
4	silver sheet	46 ± 3.1	43 ± 3.1	48 ± 2.6	0
5	PVA/CHN/STP	32 ± 2.5	30 ± 2.3	28 ± 2.2	0
6	PVA/CHN/ ß-CD	40 ± 3.2	39 ± 2.9	43 ± 3.5	0
7	PVA/CHN/ß-CD/STP	47 ± 3.4	45 ± 3.0	49 ± 3.7	0

the nanofiber mats can eliminate the pathogenic germs and absorb the undesired wound, thus accelerating the wound healing process.

The antibacterial activity of seven formulas listed in Table 3 assessed the antimicrobial properties against harmful bacteria, comprising *S. aureus*, *P. aeruginosa*, *C.* fungi (*C. albicans*), and (*A. niger*) via the disk inhibition method (expressed in the zone of inhibition (ZOI)). All formulas were much more effective on G-positive than on G-negative bacteria owing to the difference in bacterial cell walls, as shown in previous studies.[60] The results illustrated in Figure 7 indicate that all formulas

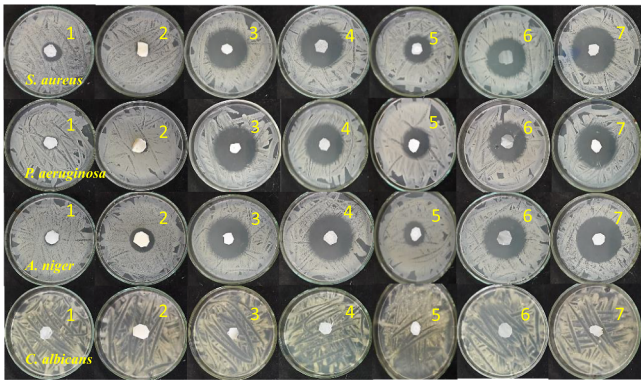

Figure 7. Antimicrobial potency of nanofiber formulations (Table 1) compared to commercial Ag sheet (sample 7) (n = 3) against (a) *S. aureus*, (b) *P. aeruginosa*, (c) *A. niger*, and (d) *C. albicans*.

have antimicrobial potency versus *P. aeruginosa*, *S. aureus*, and *A. niger* but do not possess antibacterial properties against *C. albicans*. PVA nanofiber shows the lowest antibacterial influence, but the ZOI increases with the addition of CHN. CHN can improve the antimicrobial properties of the whole mats. The ability of CHN to kill harmful organisms due to some form of electrostatic interaction between their positively charged $-NH_2$ groups and negative charges on bacterial membranes prevented bacterial cell proliferation and caused bacterium death.[61] The distinctive structural features of PVA, combined with the synergistic effects of STP, contribute significantly to the enhanced microbial resistance exhibited by these composites. In contrast to conventional silver sheets, PVA-based composites offer versatile applications and are well-suited for addressing microbial challenges in diverse environments. The remarkable antimicrobial efficacy of PVA/STP and PVA/CHN/ß-CD/STP positions them as advanced alternatives, underscoring their potential for diverse applications in combating microbial threats. Despite silver's known antimicrobial effects through the generation of reactive oxygen species (ROS), the ZOI created by PVA/CHN/ß-CD/STP surpasses that of other formulations, including the silver sheet. ß-CD has emerged as a promising antimicrobial agent, often exhibiting efficacy comparable to or even surpassing traditional antibiotics. Its unique molecular structure allows ß-CD to form inclusion complexes with various hydrophobic antimicrobial agents, enhancing their solubility and bioavailability. This property enables effective delivery of antimicrobial agents to target sites, increasing their therapeutic impact. Moreover, ß-CD itself possesses inherent antimicrobial properties, contributing to its efficacy against a broad spectrum of microorganisms. The multifaceted antimicrobial capabilities of ß-CD make it a compelling candidate for applications in antimicrobial formulations, showcasing its potential as a valuable alternative or complement to traditional antibiotics. In this case, this is normal because the efficacy of PVA/CHN/ß-CD is better than that of PVA/CHN/STP. These distinctions highlight the effectiveness of our approach, which is thoroughly substantiated in the provided data particularly in wound healing, surpassing the efficacy of traditional silver sheets.

Drawing from the aforementioned attributes, the produced nanofibers prove to be highly conducive for biomedical applications. Their expansive surface area, coupled with the potential for loading with antibacterial agents, positions them as promising candidates. Additionally, their adeptness in regulating the controlled release of these molecules in vitro from the nanofibers' surface enhances their overall medical efficacy.[62]

Based on the preceding, the resultant nanofibers are suitable for biomedical applications owing to their high surface area, ability to be loaded with antibacterial agents, and, the same time, their capability to regulate the discharge of these molecules in vitro from the nanofibers' surface to the wounds, which boosted their medical effectuality.

3.7. In Vitro Wound Healing Assay. To attain the desired percentage of wound closure of HSF cells treated with the six candidates' fabricated nanofiber formulas, specimens were added to their corresponding wells. Graphs were

https://doi.org/10.1021/acsomega.3c03146
ACS Omega 2024, 9, 10058−10068

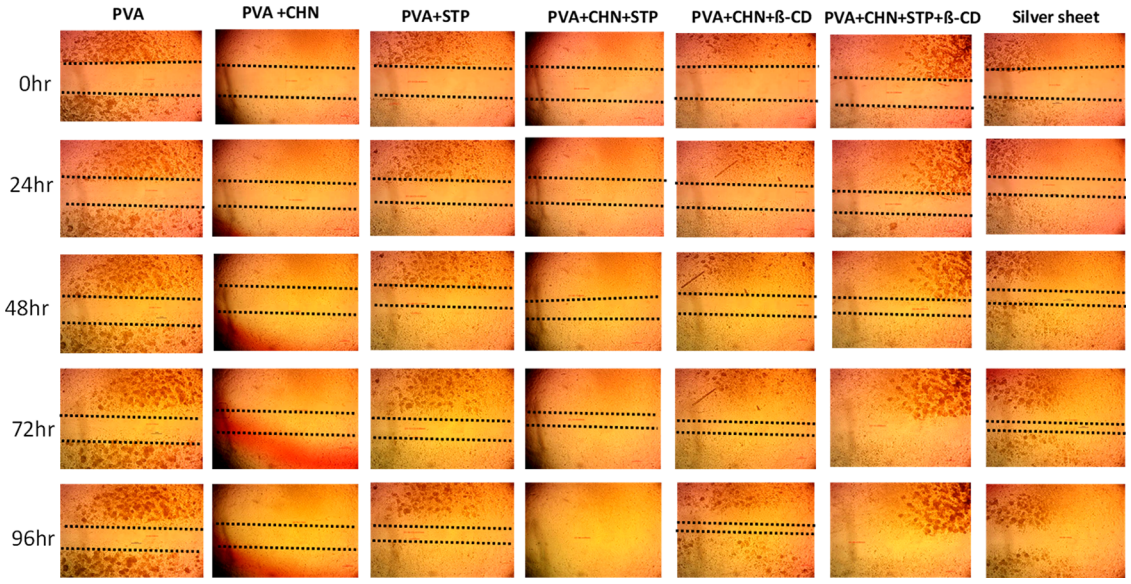

Figure 8. Wound area width of nanofiber webs versus Ag sheet at times ranging from 0 to 96 h.

Table 4. Mean ± SD of Wound Closure Width for Our Six-Nanofiber Formula Compared with the Silver Sheet

	PVA	PVA/CHN	PVA/STP	PVA/CHN/STP	PVA/CHN/ß-CD	PVA/CHN/STP /ß-CD	Ag sheet
0 h	3.7 ± 0.2	3.4 ± 0.2	4.5 ± 0.12	3.08 ± 0.02	4.1 ± 0.19	3.9 ± 0.06	3.8 ± 0.06
24 h	3.1 ± 0.2	2.2 ± 0.19	2.2 ± 0.09	2.4 ± 0.09	2.0 ± 0.07	1.6 ± 0.03	1.5 ± 0.2
48 h	2.7 ± 0.2	1.7 ± 0.01	1.4 ± 0.01	1.04 ± 0.02	1.5 ± 0.1	0.9 ± 0.06	0.6 ± 0.1
72 h	1.9 ± 0.2	1.34 ± 0.1	0.7 ± 0.2	0.5 ± 0.07	0.6 ± 0.1	0	0.11 ± 0.05
96 h	1.5 ± 0.1	1.24 ± 0.1	0.5 ± 0.06	0	0.19	0	0
wound closure (%)	59%	63%	88%	100%	95%	100%	100%

concluded at 0, 24, 48, 72, and 96 h, and the length (mm) of the width wound area was measured. As illustrated in Figure 8, the performance of six candidate formulas was evaluated by analyzing 35 wound images. Then, the study was completed, and the acquired data were used to calculate the wound area width. Figure 8 depicts the comparison of all fabricated nanofiber formulas with the PVA that reveals a nonsignificant decrease in wound width starting from 3.7 ± 0.2, reaching 1.5 ± 0.1 at 96 h with wound closure 59%; this was owing to the more excellent water absorption and moisture retention capability of hydrophilic PVA nanofiber surfaces which consequently promotes nutrient preservation and wound moistness that delay healing. However, it was noticed that after 96 h, the scratch width was reduced by the presence of the PVA/CHN with wound closure of about 63%. PVA/STP nanofiber formula, scratch wound width starts from 4.5 ± 0.12, reaching 0.5 ± 0.06 at 96 h with wound closure at 88%. The width became zero after 96 h in PVA/CHN loaded with STP, which makes the wound more sterile, which is the main factor in accelerating wound dressing.

Furthermore, in PVA/CHN/ß-CD formulas, the width significantly decreases to 0.19 at 96 h, and in PVA/CHN/STP/ß-CD, it reaches 0.9 ± 0.06 after 48 h, which disappears after 72 h. This is more significant than the Ag sheet in which the width was 0.11 ± 0.05 after 72 h and completely disappeared after 96 h, as in Table 4. So, the fabricated PVA/Cs/STP/ß-CD nanofiber formula enhanced curing in an in vitro epidermal model. Based on Figure 8 and Table 4, the wound closure proceeds at a constant rate, without significant changes except in the PVA/CHN/STP/β-CD nanofiber formula reaching almost 100% closure after 48 h, which is significantly more than the Ag sheet reaching 100% after 96 h. Moreover, these figures show that this formula substantially decreases the width of the wound area after 96 h. As reported, β-CD can enhance spinning stability in the PVA/CHN/STP/ß-CD formula.[63] Besides that, the conical shape of β-CD features a hydrophobic inner cavity and a hydrophilic outer surface, which helps to form inclusion complexes of non-covalent supramolecular hosts with a range of substances, including.[64] Because of their complexation form, which diffuses more quickly than the free drug, β-CD cavities are a fantastic way to increase the velocity of the drug solubility. The PVA/CHN/STP/β-CD combination performed the best for wound dressing within 48 h.

4. CONCLUSIONS

Utilizing the electrospinning process, nanofibrous scaffolds were fabricated, and the incorporation of STP into PVA, CHN, and ß-CD nanofibers was investigated. Morphological analysis revealed the formation of nonoriented nanonetwork scaffolds. The addition of CHN to PVA exhibited a minimal impact on morphology, with a slight increase in fiber diameter to 161.92 nm. Antibacterial assessments demonstrated broad inhibition zones of 47, 45, 49, and 0.0 mm against *S. aureus*, *P. aeruginosa*, *C. albicans*, and *A. niger*, respectively. Cell viability testing for PVA/CHN/STP/ß-CD indicated maximum viability of 96.9% at a concentration of 2000 mg/mL among the nanofibers. Wound closure assessment revealed 100% closure for the optimal PVA/CHN/STP/ß-CD composition after 72 h, outperforming the silver sheet (96 h). The combined results of cell viability, antimicrobial activity, and wound healing

https://doi.org/10.1021/acsomega.3c03146
ACS Omega 2024, 9, 10058−10068

support the potential of these nanonetworked electrospun fibers for wound dressing applications.

AUTHOR INFORMATION

Corresponding Authors

Kamel R. Shoueir − *Institute of Nanoscience & Nanotechnology, Kafrelsheikh University, 33516 Kafrelsheikh, Egypt; Institut de Chimie et Procédés Pour l'Énergie, l'Environnement et la Santé (ICPEES), CNRS, UMR 7515, Université de Strasbourg, 67087 Strasbourg, France;* orcid.org/0000-0001-7994-559X; Email: kamel_rezk@nano.kfs.edu.eg

Wafaa S. Abo El-Yazeed − *Department of Chemistry, College of Science and Humanities in Al-Kharj, Prince Sattam Bin Abdulaziz University, Al-Kharj 11942, Saudi Arabia; Chemistry Department, Faculty of Science, Mansoura University, 35516 Mansoura, Egypt;* orcid.org/0000-0002-0992-5080; Email: dr_ws2008@mans.edu.eg

Authors

Mohamed Mohsen − *Institute of Nanoscience & Nanotechnology, Kafrelsheikh University, 33516 Kafrelsheikh, Egypt*

Sara A. Abdel Gaber − *Nanomedicine Department, Institute of Nanoscience and Nanotechnology, Kafrelsheikh University, 33516 Kafrelsheikh, Egypt*

Maged El-Kemary − *Institute of Nanoscience & Nanotechnology, Kafrelsheikh University, 33516 Kafrelsheikh, Egypt*

Complete contact information is available at: https://pubs.acs.org/10.1021/acsomega.3c03146

Funding

This research received no external funding.

Notes

The authors declare no competing financial interest.

REFERENCES

(1) Todorova, K.; Mandinova, A. Novel approaches for managing aged skin and nonmelanoma skin cancer. *Adv. Drug Deliv Rev.* **2020**, *153*, 18−27.

(2) Jablonski, N.G. *Skin: A natural history*; Univ of California Press, 2008.

(3) Vass, P.; Szabó, E.; Domokos, A.; Hirsch, E.; Galata, D.; Farkas, B.; Démuth, B.; Andersen, S. K.; Vigh, T.; Verreck, G.; Marosi, G.; Nagy, Z. K. Scale-up of electrospinning technology: Applications in the pharmaceutical industry. *Wiley Interdiscip. Rev. Nanomed. Nanobiotechnol.* **2020**, *12*, No. e1611.

(4) Omer, S.; Forgách, L.; Zelkó, R.; Sebe, I. Scale-up of Electrospinning: Market Overview of Products and Devices for Pharmaceutical and Biomedical Purposes. *Pharmaceutics.* **2021**, *13*, 286.

(5) Dziemidowicz, K.; Sang, Q.; Wu, J.; Zhang, Z.; Zhou, F.; Lagaron, J. M.; Mo, X.; Parker, G. J. M.; Yu, D.-G.; Zhu, L.-M.; Williams, G. R. Electrospinning for healthcare: recent advancements. *J. Mater. Chem. B* **2021**, *9*, 939−951.

(6) Molina-santiago, C.; Pearson, J. R.; Navarro, Y.; Berlanga-clavero, M. V.; Caraballo-rodriguez, A. M.; Petras, D.; García-martín, M. L.; Lamon, G.; Haberstein, B.; Cazorla, F. M. The extracellular matrix protects Bacillus subtilis colonies from Pseudomonas invasion and modulates plant co-colonization. *Nat. Commun.* **2019**, *10*, 1919.

(7) Memic, A.; Abudula, T.; Mohammed, H. S.; Joshi navare, K.; Colombani, T.; Bencherif, S. A. Latest progress in electrospun nanofibers for wound healing applications. *ACS Appl. Bio Mater.* **2019**, *2*, 952−969.

(8) Huizing, R.; Mérida, W.; Ko, F. Impregnated electrospun nanofibrous membranes for water vapour transport applications. *J. Membr. Sci.* **2014**, *461*, 146−160.

(9) Teaima, M. H.; Abdelnaby, F. A.; Fadel, M.; El-nabarawi, M. A.; Shoueir, K. R. Synthesis of biocompatible and environmentally nanofibrous mats loaded with moxifloxacin as a model drug for biomedical applications. *Pharmaceutics* **2020**, *12*, 1029.

(10) Séon-lutz, M.; Couffin, A.-C.; Vignoud, S.; Schlatter, G.; Hébraud, A. Electrospinning in water and in situ crosslinking of hyaluronic acid/cyclodextrin nanofibers: Towards wound dressing with controlled drug release. *Carbohydr. Polym.* **2019**, *207*, 276−287.

(11) Bae, S. B.; Kim, M. H.; Park, W. H. Electrospinning and dual crosslinking of water-soluble silk fibroin modified with glycidyl methacrylate. *Polym. Degrad. Stab.* **2020**, *179*, No. 109304.

(12) Behere, I.; Ingavle, G. In vitro and in vivo advancement of multifunctional electrospun nanofiber scaffolds in wound healing applications: Innovative nanofiber designs, stem cell approaches, and future perspectives. *J. Biomed. Mater. Res. A* **2021**, *110*, 443−461, DOI: 10.1002/jbm.a.37290.

(13) Yang, Y.; Du, Y.; Zhang, J.; Zhang, H.; Guo, B. Structural and functional design of electrospun nanofibers for hemostasis and wound healing. *Advanced Fiber Materials.* **2022**, *4*, 1027−1057.

(14) Alven, S.; Buyana, B.; Feketshane, Z.; Aderibigbe, B. A. Electrospun nanofibers/nanofibrous scaffolds loaded with silver nanoparticles as effective antibacterial wound dressing materials. *Pharmaceutics.* **2021**, *13*, 964.

(15) Elsayed, M.T.; Hassan, A.A.; Abdelaal, S.A.; Taher, M.M.; Ahmed, M.K.; Shoueir, K.R. Morphological, antibacterial, and cell attachment of cellulose acetate nanofibers containing modified hydroxyapatite for wound healing utilizations. *J. Mater. Res. Technol.* **2020**, *9*, 13927−13936, DOI: 10.1016/j.jmrt.2020.09.094.

(16) Lemraski, E. G.; Jahangirian, H.; Dashti, M.; Khajehali, E.; Sharafinia, S.; Rafiee-moghaddam, R.; Webster, T. J. Antimicrobial double-layer wound dressing based on chitosan/polyvinyl alcohol/copper: In vitro and in vivo assessment. *Int. J. Nanomedicine* **2021**, *16*, 223−235.

(17) Ghomi, E. R.; Lakshminarayanan, R.; Chellappan, V.; Verma, N. K.; Chinnappan, A.; Neisiany, R. E.; Amuthavalli, K.; Poh, Z. S.; Wong, B. H. S.; Dubey, N. Electrospun aligned PCL/gelatin scaffolds mimicking the skin ECM for effective antimicrobial wound dressings. *Adv. Fiber Mater.* **2023**, *5*, 235−251.

(18) Dodero, A.; Schlatter, G.; Hébraud, A.; Vicini, S.; Castellano, M. Polymer-free cyclodextrin and natural polymer-cyclodextrin electrospun nanofibers: A comprehensive review on current applications and future perspectives. *Carbohydr. Polym.* **2021**, *264*, No. 118042.

(19) Campa-siqueiros, P. I.; Madera-santana, T. J.; Castillo-ortega, M. M.; López-cervantes, J.; Ayala-zavala, J. F.; Ortiz-vazquez, E. L. Electrospun and co-electrospun biopolymer nanofibers for skin wounds on diabetic patients: an overview. *RSC Adv.* **2021**, *11*, 15340−15350.

(20) Alven, S.; Aderibigbe, B. A. Fabrication of Hybrid Nanofibers from Biopolymers and Poly (Vinyl Alcohol)/Poly (ε-Caprolactone) for Wound Dressing Applications. *Polymers* **2021**, *13*, 2104.

(21) Shokraei, S.; Mirzaei, E.; Shokraei, N.; Derakhshan, M. A.; Ghanbari, H.; Faridi-majidi, R. Fabrication and characterization of chitosan/kefiran electrospun nanofibers for tissue engineering applications. *J. Appl. Polym. Sci.* **2021**, *138*, 50547.

(22) Wu, X.; Li, H. Incorporation of Bioglass Improved the Mechanical Stability and Bioactivity of Alginate/Carboxymethyl Chitosan Hydrogel Wound Dressing. *ACS Appl. Bio Mater.* **2021**, *4*, 1677−1692.

(23) He, J.; Liang, Y.; Shi, M.; Guo, B. Anti-oxidant electroactive and antibacterial nanofibrous wound dressings based on poly (ε-caprolactone)/quaternized chitosan-graft-polyaniline for full-thickness skin wound healing. *Chemical Engineering Journal.* **2020**, *385*, No. 123464.

(24) Shaban, N. Z.; Aboelsaad, A. M.; Shoueir, K. R.; Abdulmalek, S. A.; Awad, D.; Shaban, S. Y.; Mansour, H. Chitosan-based

dithiophenolato nanoparticles: Preparation, mechanistic information of DNA binding, antibacterial and cytotoxic activities. *J. Mol. Liq.* **2020**, *318*, No. 114252.
(25) Li, Z.; Meng, Z.; Zhao, Z. Silk fibroin nanofibrous scaffolds incorporated with microRNA-222 loaded chitosan nanoparticles for enhanced neuronal differentiation of neural stem cells. *Carbohydr. Polym.* **2022**, *277*, No. 118791.
(26) Shoueir, K. R. Green microwave synthesis of functionalized chitosan with robust adsorption capacities for Cr (VI) and/or RHB in complex aqueous solutions. *Environ. Sci. Pollut. Res.* **2020**, *27*, 33020−33031.
(27) Shawky, S.; El-shafai, N. M.; El-mehasseb, I. M.; Shoueir, K. R.; El-kemary, M. A. Spectroscopic study of self-assembly of anti-hepatitis C virus sofosbuvir drug with bio-polymeric nanoparticles for improving the drug release effect. *Spectrochim Acta A Mol. Biomol Spectrosc.* **2021**, *261*, No. 120008.
(28) Shoueir, K.R.; El-Desouky, N.; Rashad, M.M.; Ahmed, M.K.; Janowska, I.; El-Kemary, M. Chitosan based-nanoparticles and nanocapsules: Overview, physicochemical features, applications of a nanofibrous scaffold, and bioprinting. *Int. J. Biol. Macromol.* **2020**, *167*, 1176−1197, DOI: 10.1016/j.ijbiomac.2020.11.072.
(29) Ismail, N.; Shoueir, K. R.; Toson, E. A. Hepatoprotective activity and free radical scavenging against induction of CCl4 in an experimental model using dendronaphthya crude extract loaded chitosan nanocarrier. *J. Drug Deliv Sci. Technol.* **2021**, *66*, No. 102906.
(30) El-Okaily, M. S.; El-Rafei, A. M.; Basha, M.; Ghani, N. T. A.; El-Sayed, M. M. H.; Bhaumik, A.; Mostafa, A. A. Efficient drug delivery vehicles of environmentally benign nano-fibers comprising bioactive glass/chitosan/polyvinyl alcohol composites. *Int. J. Biol. Macromol.* **2021**, *182*, 1582−1589.
(31) Hashmi, M.; Ullah, S.; Kim, I. S. Electrospun Momordica charantia incorporated polyvinyl alcohol (PVA) nanofibers for antibacterial applications. *Mater. Today Commun.* **2020**, *24*, No. 101161.
(32) Lim, Y. R. I.; Preshaw, P. M.; Lim, L. P.; Ong, M. M. A.; Lin, H.-S.; Tan, K. S. Pterostilbene complexed with cyclodextrin exerts antimicrobial and anti-inflammatory effects. *Sci. Rep.* **2020**, *10*, 9072.
(33) Gao, S.; Liu, Y.; Jiang, J.; Li, X.; Zhao, L.; Fu, Y.; Ye, F. Encapsulation of thiabendazole in hydroxypropyl-β-cyclodextrin nanofibers via polymer-free electrospinning and its characterization. *Pest Manag Sci.* **2020**, *76*, 3264−3272.
(34) Dos Santos, J. P.; da Rosa Zavareze, E.; Dias, A. R. G.; Vanier, N. L. Immobilization of xylanase and xylanase−β-cyclodextrin complex in polyvinyl alcohol via electrospinning improves enzyme activity at a wide pH and temperature range. *Int. J. Biol. Macromol.* **2018**, *118*, 1676−1684.
(35) Tian, B.; Liu, Y.; Liu, J. Cyclodextrin as a magic switch in covalent and non-covalent anticancer drug release systems. *Carbohydr. Polym.* **2020**, *242*, No. 116401.
(36) Pushpalatha, R.; Selvamuthukumar, S.; Kilimozhi, D. Cross-linked, cyclodextrin-based nanosponges for curcumin delivery-Physicochemical characterization, drug release, stability and cytotoxicity. *J. Drug Deliv Sci. Technol.* **2018**, *45*, 45−53.
(37) Unnithan, A. R.; Gnanasekaran, G.; Sathishkumar, Y.; Lee, Y. S.; Kim, C. S. Electrospun antibacterial polyurethane−cellulose acetate−zein composite mats for wound dressing. *Carbohydr. Polym.* **2014**, *102*, 884−892.
(38) Khalek, M. A. A.; Gaber, S. A. A.; El-domany, R. A.; El-kemary, M. A. Photoactive electrospun cellulose acetate/polyethylene oxide/methylene blue and trilayered cellulose acetate/polyethylene oxide/silk fibroin/ciprofloxacin nanofibers for chronic wound healing. *Int. J. Biol. Macromol.* **2021**, *193*, 1752−1766.
(39) Yasin, G.; Nasr, M.; Gaber, S. A. A.; Hüttenberger, D.; Fadel, M. Response surface methodological approach for optimization of photodynamic therapy of onychomycosis using chlorin e6 loaded nail penetration enhancer vesicles. *J. Photochem. Photobiol. B* **2022**, *232*, No. 112461.
(40) El-kemary, B. M.; El-borady, O. M.; Abdel gaber, S. A.; Beltagy, T. M. Role of nano-zirconia in the mechanical properties improvement of resin cement used for tooth fragment reattachment. *Polym. Compos.* **2021**, *42*, 3307−3319.
(41) Ibrahim, A.; Abdel gaber, S. A.; Fawzi kabil, M.; Ahmed-farid, O. A. H.; Hirsch, A. K. H.; El-sherbiny, I. M.; Nasr, M. Baicalin lipid nanocapsules for treatment of glioma: Characterization, mechanistic cytotoxicity, and pharmacokinetic evaluation. *Expert Opin Drug Delivery* **2022**, *19*, 1549−1560.
(42) Abdel Gaber, S. A.; Stepp, H.; Abdel Kader, M. H.; Lindén, M. Mesoporous silica nanoparticles boost aggressive cancer response to hydrophilic chlorin e6-mediated photodynamic therapy. *Cancer Nanotechnol.* **2023**, *14*, 67.
(43) Koosha, M.; Raoufi, M.; Moravvej, H. One-pot reactive electrospinning of chitosan/PVA hydrogel nanofibers reinforced by halloysite nanotubes with enhanced fibroblast cell attachment for skin tissue regeneration. *Colloids Surf. B Biointerfaces.* **2019**, *179*, 270−279.
(44) Fan, J.-P.; Luo, J.-J.; Zhang, X.-H.; Zhen, B.; Dong, C.-Y.; Li, Y.-C.; Shen, J.; Cheng, Y.-T.; Chen, H.-P. A novel electrospun β-CD/CS/PVA nanofiber membrane for simultaneous and rapid removal of organic micropollutants and heavy metal ions from water. *Chemical Engineering Journal.* **2019**, *378*, No. 122232.
(45) Shoueir, K.; El-Sheshtawy, H.; Misbah, M.; El-Hosainy, H.; El-Mehasseb, I.; El-kemary, M. Fenton-like nanocatalyst for photo-degradation of methylene blue under visible light activated by hybrid green DNSA@Chitosan@$MnFe_2O_4$. *Carbohydr. Polym.* **2018**, *197*, 17−28, DOI: 10.1016/j.carbpol.2018.05.076.
(46) Hsiung, E.; Celebioglu, A.; Kilic, M. E.; Durgun, E.; Uyar, T. Ondansetron/Cyclodextrin inclusion complex nanofibrous webs for potential orally fast-disintegrating antiemetic drug delivery. *Int. J. Pharm.* **2022**, *623*, No. 121921.
(47) Maslakci, N. N.; Eren, E.; Kocer, K. N.; Cevikbas, H.; Ulusoy, S.; Bicer, A.; Cin, G. T.; Oksuz, A. U. Controlled drug release characteristics and antibacterial influence of streptomycin sulfate-loaded PMMA/PEO/bis-chalcone derivatives-based fibers. *Mater. Today Commun.* **2022**, *31*, No. 103784.
(48) Celebioglu, A.; Yildiz, Z. I.; Uyar, T. Electrospun crosslinked poly-cyclodextrin nanofibers: Highly efficient molecular filtration thru host-guest inclusion complexation. *Sci. Rep.* **2017**, *7*, 7369.
(49) Ranjbar-mohammadi, M.; Sa'di, V.; Moezzi, M.; Saghafi, R. Fabrication and Characterization of Antibacterial Suture Yarns Containing PLA/Tetracycline Hydrochloride-PVA/Chitosan Nanofibers. *Fibers Polym.* **2022**, *23*, 1538−1547.
(50) Celebioglu, A.; Uyar, T. Cyclodextrin nanofibers by electrospinning. *Chemical Communications.* **2010**, *46*, 6903−6905.
(51) Celebioglu, A.; Saporito, A. F.; Uyar, T. Green Electrospinning of Chitosan/Pectin Nanofibrous Films by the Incorporation of Cyclodextrin/Curcumin Inclusion Complexes: pH-Responsive Release and Hydrogel Features. *ACS Sustain Chem. Eng.* **2022**, *10*, 4758−4769.
(52) Celebioglu, A.; Uyar, T. Fast dissolving oral drug delivery system based on electrospun nanofibrous webs of cyclodextrin/ibuprofen inclusion complex nanofibers. *Mol. Pharmaceutics* **2019**, *16*, 4387−4398.
(53) Hsiung, E.; Celebioglu, A.; Chowdhury, R.; Kilic, M. E.; Durgun, E.; Altier, C.; Uyar, T. Antibacterial nanofibers of pullulan/tetracycline-cyclodextrin inclusion complexes for Fast-Disintegrating oral drug delivery. *J. Colloid Interface Sci.* **2022**, *610*, 321−333.
(54) Abasalta, M.; Asefnejad, A.; Khorasani, M. T.; Saadatabadi, A. R.; Irani, M. Adsorption and sustained release of doxorubicin from N-carboxymethyl chitosan/polyvinyl alcohol/poly (ε-caprolactone) composite and core-shell nanofibers. *J. Drug Deliv Sci. Technol.* **2022**, *67*, No. 102937.
(55) Hussein, M. A. M.; Guler, E.; Rayaman, E.; Cam, M. E.; Sahin, A.; Grinholc, M.; Mansuroglu, D. S.; Sahin, Y. M.; Gunduz, O.; Muhammed, M. Dual-drug delivery of Ag-chitosan nanoparticles and phenytoin via core-shell PVA/PCL electrospun nanofibers. *Carbohydr. Polym.* **2021**, *270*, No. 118373.
(56) Kadkhodaie-elyaderani, A.; De lama-odría, M. D. C.; Rivas, M.; Martínez-rovira, I.; Yousef, I.; Puiggalí, J.; Del valle, L. J. Medicated Scaffolds Prepared with Hydroxyapatite/Streptomycin Nanoparticles

https://doi.org/10.1021/acsomega.3c03146
ACS Omega 2024, 9, 10058−10068

Encapsulated into Polylactide Microfibers. *Int. J. Mol. Sci.* **2022**, *23*, 1282.
(57) Ibrahim, H. M.; Reda, M. M.; Klingner, A. Preparation and characterization of green carboxymethylchitosan (CMCS)−Polyvinyl alcohol (PVA) electrospun nanofibers containing gold nanoparticles (AuNPs) and its potential use as biomaterials. *Int. J. Biol. Macromol.* **2020**, *151*, 821−829.
(58) Abdelnaby, M. A.; Shoueir, K. R.; Ghazy, A. A.; Abdelhamid, S. M.; El kemary, M. A.; Mahmoud, H. E.; Baraka, K.; Abozahra, R. R. Synthesis and evaluation of metallic nanoparticles-based vaccines against Candida albicans infections. *J. Drug Deliv Sci. Technol.* **2022**, *68*, No. 102862.
(59) Teaima, M. H.; Elasaly, M. K.; Omar, S. A.; El-nabarawi, M. A.; Shoueir, K. R. Wound healing activities of polyurethane modified chitosan nanofibers loaded with different concentrations of linezolid in an experimental model of diabetes. *J. Drug Deliv Sci. Technol.* **2022**, *67*, No. 102982.
(60) Elksass, S.; Alkabes, H. A.; El-kemary, N. M.; El-kelany, K. E.; El-kemary, M. Anti-bacterial and multi-functional smart wearable sensor based on organo-hydrogel for diagnosis of the anterior cruciate ligament injuries, and sensing glove for rehabilitation of joints motion. *Mater. Today Commun.* **2022**, *32*, No. 104131.
(61) Gulzar, S.; Tagrida, M.; Nilsuwan, K.; Prodpran, T.; Benjakul, S. Electrospinning of gelatin/chitosan nanofibers incorporated with tannic acid and chitooligosaccharides on polylactic acid film: Characteristics and bioactivities. *Food Hydrocoll.* **2022**, *133*, No. 107916.
(62) Mosaad, K. E.; Shoueir, K. R.; Dewidar, M. M. Fabrication of Multifunctional Wound Dressing Composite Biomaterials Composed of Ag/Mg-Hydroxyapatite Doped Electrospun Poly (Vinyl Alcohol) Nanofibers for Skin Tissue Regeneration. *J. Clust. Sci.* **2021**, *34*, 135−146.
(63) Topuz, F.; Uyar, T. Electrospinning of cyclodextrin nanofibers: the effect of process parameters. *J. Nanomater.* **2020**, *2020*, No. 7529306.
(64) Aytac, Z.; Yildiz, Z. I.; Kayaci-senirmak, F.; Tekinay, T.; Uyar, T. Electrospinning of cyclodextrin/linalool-inclusion complex nanofibers: Fast-dissolving nanofibrous web with prolonged release and antibacterial activity. *Food Chem.* **2017**, *231*, 192−201.

https://doi.org/10.1021/acsomega.3c03146
ACS Omega 2024, 9, 10058−10068